Journal of Materials Chemistry B

PAPER

View Article Online
View Journal | View Issue

Cite this: *J. Mater. Chem. B*, 2019, 7, 7704

A non-enzymatic electrochemical biosensor based on Au@PBA(Ni–Fe):MoS_2 nanocubes for stable and sensitive detection of hydrogen peroxide released from living cells†

Wang Zhang, Chao Wang, Lihao Guan, Meihong Peng, Kai Li* and Yuqing Lin *

Received 21st September 2019,
Accepted 13th November 2019

DOI: 10.1039/c9tb02059d

rsc.li/materials-b

Hydrogen peroxide (H_2O_2) is the main product of enzymatic reactions and plays an important role in biological processes. The detection of H_2O_2 inside organisms or cells is critical. Here, we report a nickel–iron Prussian blue analogue nanocube doped with molybdenum disulfide and Au nanoparticles (Au@PBA(Ni–Fe):MoS_2) as an electrochemical sensing material for the stable detection of H_2O_2 in neutral solutions for a long time. First, the Prussian blue analogue (PBA(Ni–Fe)) is synthesized by a simple charge-assembly technology, and then etched into PBA(Ni–Fe):MoS_2 hollow nanocubes by a high-temperature hydrothermal reaction. Finally, Au nanoparticles are reduced inside the PBA(Ni–Fe):MoS_2 *in situ* to generate Au@PBA(Ni–Fe):MoS_2 nanocubes. Ni-doping enhances the nanocube's stability in neutral solutions; as a result, the sensor can maintain a stable current response towards H_2O_2 reduction for more than 1 h. The sensing material can meet the needs of a long-time test. The introduction of Au enhances the electron transfer efficiency, which endows the sensor with good reduction ability for H_2O_2 at 0 V over a wide linear range (0.5–200 μM and 210–3000 μM) and with a low detection limit (0.23 μM (S/N = 3)), which fulfills the requirements for the detection of H_2O_2 in a biological system. The sensor can sense H_2O_2 released from cells stimulated by ascorbic acid. Au@PBA(Ni–Fe):MoS_2 provides good guidance for the future development of efficient biosensors to be applied in cell biology.

Introduction

Hydrogen peroxide (H_2O_2) is the main product of enzymatic reactions and plays an important role in biological processes.[1] The compound is one of the most important representatives of oxygen activity, and is produced by cell metabolism, being widely present during cell growth and signalling.[2] The concentration of H_2O_2 in cells can be used as a health index. However, H_2O_2 can cause many diseases, such as tumours, cardiac diseases, Alzheimer's disease and more when present in abnormal concentrations.[2] Meanwhile, the H_2O_2 concentration level is an important biological parameter for detecting myocardial infarction, Parkinson's disease and cancer. To date, various methods such as chemiluminescence, fluorescence, photocolorimetry, colorimetry and electrochemistry have been used to detect H_2O_2.[3–8] Among these methods, electrochemical technology presents high selectivity, simple operation and low cost, and is common in the field of analysis. There are many types of H_2O_2 sensors prepared by this technology. Traditional enzymatic sensors possess high selectivity for H_2O_2, but their poor stability, high cost and insensitivity make them unsuitable for commercial applications.[9] Traditional non-enzymatic sensors consist of low-cost and stable materials, including hydrogels, noble metals, non-precious metals, redox-based conducting polymers, functionalized metal–organic frameworks and metal-free carbon-based materials, but they still exhibit poor selectivity and low sensitivity.[10–15] It is necessary to detect H_2O_2 in the biological environment using a non-enzymatic sensor.

Prussian blue (PB) and Prussian blue analogues (PBAs) are formed by the coordination of metal ion centres with cyanide.[16] The metal ions have multiple valence states and coordination ions, resulting in a variety of compositions and controllable morphology of PBAs.[17] The face of the PB nanocube consists of iron and ferrous ions. Each ferrous ion is surrounded by carbon atoms, and each iron is surrounded by nitrogen atoms.[18] When the iron ions in a PB nanocube are oxidized to ferrous ions, the electron loss can result in the transfer to and reduction of

Department of Chemistry, Capital Normal University, Beijing, 100048, China. E-mail: likai@cnu.edu.cn, linyuqing@cnu.edu.cn; Fax: +86 1068903047; Tel: +86 1068903047

† Electronic supplementary information (ESI) available: TEM and SEM images of PBA(Ni–Fe), PBA(Ni–Fe):MoS_2, SEM images of Au@PBA(Ni–Fe):MoS_2 before and after the electrochemical test, EDS spectrum of Au@PBA(Ni–Fe):MoS_2, FT-IR spectra and Raman spectra of PBA(Ni–Fe), PBA(Ni–Fe):MoS_2, Au@PBA(Ni–Fe):MoS_2, and EIS behaviors of PBA(Ni–Fe)/GCE, Au@PBA(Ni–Fe)/GCE, PBA(Ni–Fe):MoS_2/GCE and Au@PBA(Ni–Fe):MoS_2/GCE. See DOI: 10.1039/c9tb02059d

H_2O_2.[19] PB and PBAs have been used in many fields due to their unique electronic properties, including catalysis, energy storage, chemo/biosensors, and environmental and food applications.[20–24] PB is expressed as an artificial enzyme peroxidase owing to its excellent electrochemical catalytic ability and selectivity, and it can be used to detect H_2O_2.[25] However, it is difficult for electrons to be excited from the valence band to the conduction band because PBA materials possess semiconductor properties.[26,27] Therefore, the majority of sensors based on PB materials have poor sensitivity and a high detection limit.[28,29] Furthermore, for the electrochemical process, the conductivity and electron transport rate of PB materials are not satisfactory.[30,31,32] Consequently, as a sensor to detect H_2O_2, the electrical conductivity and stability of PB need to be enhanced.

Many reports have stated that nanosized molybdenum sulfide (MoS_2) holds promise as a high-performance catalyst for the hydrogen evolution reaction and the oxygen reduction reaction and have presented the potential for the construction of electrocatalytic biosensors due to the material's excellent electrocatalytic properties. However, conventional MoS_2 sensors cannot meet the demands of electrochemical detection because of the low sensitivity of an undefined surface.[33]

Herein, we report Au@PBA(Ni–Fe):MoS_2 as a sensing material to construct a highly stable non-enzymatic electrochemical biosensor for the detection of H_2O_2 released from cells. As shown in Scheme 1, first, a nickel-doped PBA (PBA(Ni–Fe)) was prepared by the charge-assembly strategy. The addition of nickel enhances the stability of the PBA and can maintain a constant PBA response for a long time in neutral solution. Afterwards, the PBA was etched into a hollow structure (PBA(Ni–Fe):MoS_2), and Au nanoparticles were grown *in situ* (Au@PBA(Ni–Fe):MoS_2). PBA(Ni–Fe):MoS_2 nanocubes provide large active load regions for Au nanoparticles, while Au nanoparticles significantly enhance the electron transfer rate and increase the response signal. The synergistic effect of Au and MoS_2 improves the sensitivity of the sensor. Compared to conventional nanocomposite-modified electrodes, the working electrode potential of the Au@PBA(Ni–Fe):MoS_2 modified glass carbon electrode is significantly improved (approximately 0.2 V *vs.* Ag/AgCl), which helps to avoid interference from reducing substances such as ascorbic acid. Through the synergistic action of PBA(Ni–Fe):MoS_2 and Au nanoparticles, the prepared H_2O_2 biosensor could detect trace H_2O_2 at a working potential of 0 V, with excellent selectivity and high sensitivity.

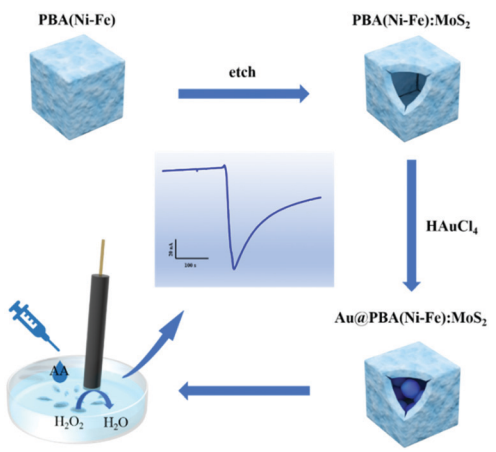

Scheme 1 Schematic illustrating the preparation process of the Au@PBA(Ni–Fe):MoS_2 nanocubes and their electrochemical applications.

Experimental section

Reagents and apparatus

H_2O_2, ascorbic acid (AA), glutamic acid (Glu), glycine (Gly), dopamine (DA), uric acid (UA), L-cysteine (L-Cys), and *N*,*N*-dimethylformamide (DMF) were purchased from Sigma (Shanghai, China). $Ni(NO_3)_2{\cdot}6H_2O$, $K_3[Fe(CN)_6]$, ammonium thiomolybdate ($H_8MoN_2S_4$), Pluronic F127, chloroauric acid ($HAuCl_4$), trisodium citrate dihydrate ($C_6H_5Na_3O_7{\cdot}2H_2O$), potassium chloride (KCl) and monopotassium phosphate were purchased from Beijing Chemical Reagent Company. All the chemicals were used as received without further purification. A Milli-Q plus water purification system (18 MΩ, Milli-pore Co., Ltd, USA) was used to obtain ultra-pure water, which was used in all parts related to the aqueous environment.

The TEM, HRTEM and mapping images were recorded on a JEM-2100F TEM (Japan). The SEM images and energy dispersive X-ray spectroscopy (EDS) mapping were collected on a Hitachi SU8010. Samples for SEM images were deposited on a carbon conductive adhesive. Wide-angle XRD patterns were recorded on a Bruker D8 advance powder diffractometer using Cu Kα radiation. Raman spectra were obtained using a Renishaw Raman system model 1000 spectrometer operating with a 20 mW air-cooled argon ion laser (785 nm) as the excitation light source. FT-IR spectra were recorded on a TENSOR-27 (Bruker) at room temperature. X-ray photoelectron spectra (XPS) were recorded on an ESCALAB 250 spectrometer, using a standard Al Kα radiation exciting source. All binding energies were referenced to the C 1s binding energy of adventitious carbon contamination taken to 284.7 eV.

Cyclic voltammograms (CV) and typical current–time curves were recorded on a CHI 1000c electrochemical workstation (CH Instruments, Shanghai, China).

Preparation of Au@PBA(Ni–Fe):MoS_2

Firstly, 0.1745 g of (0.03 M) $Ni(NO_3)_2{\cdot}6H_2O$ and 0.2647 g of (0.045 M) $C_6H_5Na_3O_7{\cdot}2H_2O$ were dissolved in 20 mL of deionized water. Secondly, 0.1317 g of (0.04 M) $K_3[Fe(CN)_6]$ was added into 10 mL of deionized water. Then the above two solutions were mixed together and stewed for 20 h at room temperature. Uniform PBA(Ni–Fe) nanocubes were synthesized. To etch the nanocubes hydrothermally, 30 mg of the above as-prepared PBA(Ni–Fe) nanocubes and 10 mg of $H_8MoN_2S_4$ were dissolved in 30 mL of DMF, and then subjected to ultrasonic treatment for 15 min. The mixture was transferred into a 50 mL autoclave and reacted at 210 °C for 20 h. The products were washed with deionized water and ethanol three times and dried at 60 °C overnight. Uniform PBA(Ni–Fe):MoS_2 nanocubes were synthesized. Au@PBA(Ni–Fe):MoS_2 was prepared from PBA(Ni–Fe):MoS_2 nanocubes. To 5 mg of PBA(Ni–Fe):MoS_2

dissolved in 1 mL of deionized water and 20 mg of Pluronic F127 dissolved in 5 mL of deionized water, 1 mL of $HAuCl_4$ (10 mM) was added and mixed. After stirring for 30 min, 1.4 mL of AA (10 mM) was added to reduce $HAuCl_4$. After continually stirring for 1 h, the products were centrifuged at 8000 rpm for 5 min and washed with deionized water and ethanol, and then dried at 40 °C overnight. Au@PBA(Ni–Fe):MoS_2 was obtained.

Fabrication of different modified electrodes

Firstly, a bare glassy carbon electrode (GCE) was polished with alumina powder of size 1 and 0.05 μm in an electrode polishing machine. Thereafter, it was ultrasonically treated in absolute ethanol and double distilled water for 1 min, respectively. This could remove the oxidation film and a few impurities adsorbed from air. The electrochemical behavior was characterized to verify whether it was polished clean. Subsequently, 5 μL of Au@PBA(Ni–Fe):MoS_2 suspension (2.0 mg mL^{-1}) was carefully dropped on the surface of the freshly polished GCE, and the electrode was dried in air at room temperature. Ultimately, Au@PBA(Ni–Fe):MoS_2/GCE was prepared. PBA(Ni–Fe)/GCE and PBA(Ni–Fe):MoS_2/GCE were prepared by the same procedures.

Cell culture

Cervical cancer cells (HeLa) were cultured in medium (430167) with 84% H-DMEM, 15% fetal bovine serum, 1% penicillin and streptomycin at 37 °C in a humidified incubator (95% air with 5% CO_2). It was kept in the incubator for 24 h to allow the cells to adhere and loosely bind. The number of cells (4×10^6) was counted using a hemocytometer.

Electrochemical determination of H_2O_2 released by living cells

After culturing HeLa cells for 24 h at the interface, the plates were taken out and washed with sterile phosphate buffer to remove the medium. Subsequently, 500 μL of 100 mM PBS (containing 0.1 M KCl, pH 7.4) was injected into the culture dish as the electrolyte. The current response was recorded when AA (0.1 mM) was injected for quantitative detection of H_2O_2 released from cells.

Results and discussion

Characterization of Au@PBA(Ni–Fe):MoS_2

TEM was used to characterize the morphology of the Au@PBA-(Ni–Fe):MoS_2. Fig. 1A and B show that Au@PBA(Ni–Fe):MoS_2 is a hollow cubic structure with a size of approximately 120 nm. As presented in Fig. S1 A–H (ESI†), TEM and SEM images of PBA(Ni–Fe) and PBA(Ni–Fe):MoS_2 reveal that during the synthesis of Au@PBA(Ni–Fe):MoS_2, the size remains unchanged. Ammonium thiomolybdate etches PBA(Ni–Fe) from the inside to different extents. The lattice fringes were used to measure the interplanar spacing of the Au nanoparticles on the Au@P-BA(Ni–Fe):MoS_2 nanocubes (Fig. 1C), and the calculated values were approximately 0.23 nm and 0.20 nm, which corresponded to the (111) and (200) planes of Au, respectively. This result was consistent with the result from XRD for the crystal facets (Fig. 2A).

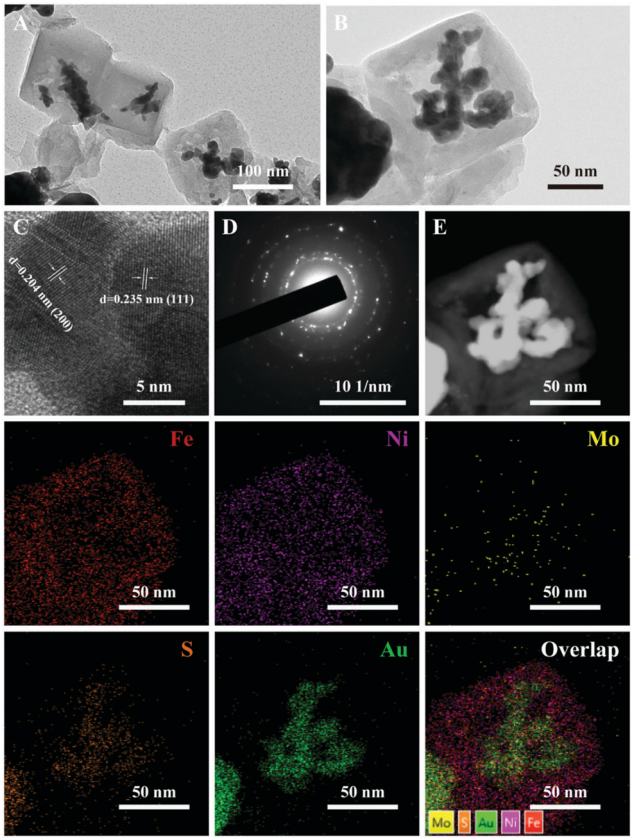

Fig. 1 (A and B) TEM images, (C) HRTEM image, (D) SAED pattern, and (E) mapping images of Au@PBA(Ni–Fe):MoS_2.

Furthermore, the SAED pattern in Fig. 1D confirms that the prepared Au@PBA(Ni–Fe):MoS_2 nanocubes are polycrystals. The composition of the Au@PBA(Ni–Fe):MoS_2 nanocubes can be investigated by EDS. As shown in Fig. S1L (ESI†), the elemental peaks were assigned to C, Ni, Fe, Au, Mo and S as expected. TEM mapping was used to determine the corresponding distribution of the five elements (Fig. 1E). It is apparent that Ni and Fe are elements uniformly distributed throughout the surface of the nanocube. The structure of the nanocubes remained stable during the preparation of Au@PBA(Ni–Fe):MoS_2. The Mo and S elements mainly correlate with the etching interface. By charge assembly, Au nanoparticles combined with PBA(Ni–Fe):MoS_2. Furthermore, the etching interface of PBA(Ni–Fe):MoS_2 contains S ions, which can be combined with Au nanoparticles through Au–S bonds. Combined with the mappings, Fig. 1A and B reveal that the light-grey block is PBA(Ni–Fe):MoS_2, and the black region inside the block represents the Au nanoparticles, indicating that the Au nanoparticles and PBA(Ni–Fe):MoS_2 are successfully combined. The amount of Au nanoparticles contained in each block is different, which is also verified by the SEM images (Fig. S1I and J, ESI†).

XRD was used to investigate the crystal structures of three nanocubes. As shown in Fig. 2A, the three kinds of nanocubes all present a series of diffraction peaks located at 17.3°, 24.2°, 35.2° and 39.4°. These four peaks correspond to the (200), (220), (400) and (420) crystalline planes of $KNi(Fe(CN)_6)$ (PDF# 51-1897).[34] This result demonstrates that during the synthesis of Au@PBA(Ni–Fe):MoS_2,

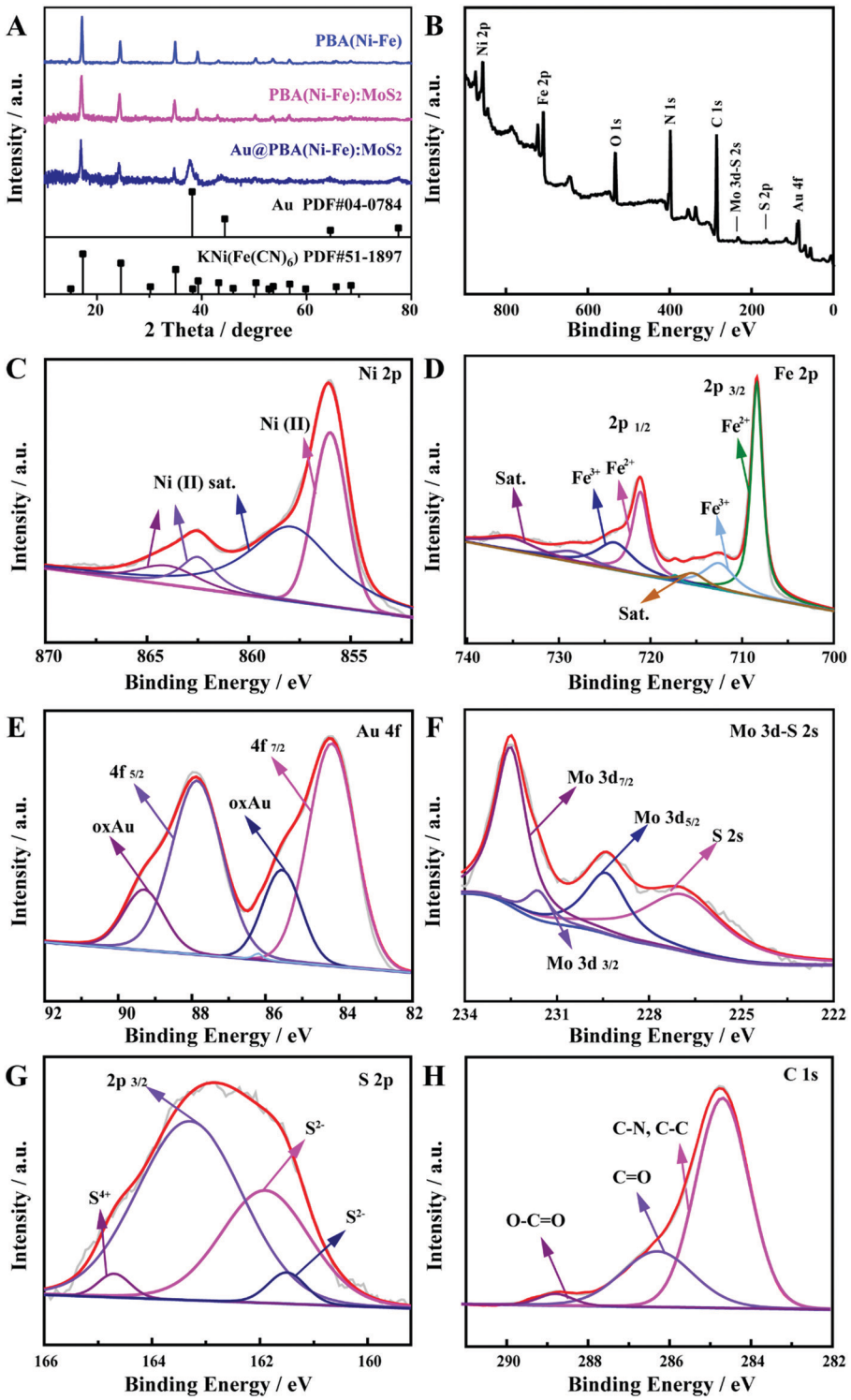

Fig. 2 (A) XRD patterns, (B) XPS survey spectrum of Au@PBA(Ni–Fe):MoS_2, (C–H) XPS spectra of Ni 2p, Fe 2p, Au 4f, Mo 3d, S 2s, S 2p and C 1s of Au@PBA:MoS_2 nanocubes, respectively.

the nanocubes maintain a stable Prussian-blue-like crystal structure. In addition, the pattern for Au@PBA(Ni–Fe):MoS_2 exhibits several peaks that can be well-indexed to Au.[34,35] The four peaks at 38.2°, 44.4°, 64.5° and 77.6° indicated the (111), (200), (220) and (311) planes of Au (PDF# 04-0784).[36] These data proved that the Au nanoparticles were satisfactorily combined with and deposited onto PBA(Ni–Fe):MoS_2. However, the diffraction peaks of MoS_2 cannot be observed, suggesting that MoS_2 may exist inside of the PBA(Ni–Fe) frame, rather than on the surface.[37] This notion is consistent with the results obtained from the mapping images of Mo and S atoms.

X-ray photoelectron spectroscopy (XPS) was used to analyse the elementary composition, elemental chemical state and electronic state of the Au@PBA(Ni–Fe):MoS_2 surface. The survey spectrum indicated that the surface of Au@PBA(Ni–Fe):MoS_2 mainly contained Ni, Fe, and Au, while trace Mo and S exist on the surface (Fig. 2B). The presence of the O 1s peak indicates that surface oxidation took place after the exposure of the sample to the atmosphere. Combined with the results of EDX (Fig S1A, ESI†), the XPS spectra indicated that Mo and S elements mainly existed within the interior of PBA nanocubes. Representative spectra of the Ni 2p, Fe 2p, Au 4f, Mo 3d, S 2p and C 1s are shown in Fig. 2C–H. The Ni 2p spectrum exhibits a main peak and some satellite peaks (Fig. 2C). The peak near 856 eV corresponds to the Ni(II) species, and the other peaks can be assigned to the satellite peaks of the corresponding Ni species. The Fe 2p spectrum (Fig. 2D) exhibits two contributions, $2p_{1/2}$ and $2p_{3/2}$ located at 721 eV and 708.4 eV, respectively, which resulted from the spin–orbital splitting (SOS), and their intensity ratio is 1 : 2. The two peaks were characteristic of the Fe^{2+} oxidation state.[38–40] The Au 4f spectrum exhibits two chemical environments for Au atoms. The peaks located at 84.2 eV and 87.9 eV (Fig. 2E) are respectively assigned to $4f_{7/2}$ and $4f_{5/2}$, and their intensity ratio is 4 : 3,[41] whereas the peaks at 85.5 and 89.3 are ascribed to the $4f_{7/2}$ and $4f_{5/2}$ photoelectrons of oxidized Au.[42] The Mo 3d–S 2s spectrum evidences the Mo $3d_{5/2}$ orbital at 229.0 eV and Mo $3d_{7/2}$ at 232.2 eV (Fig. 2F). The peak at 231.5 eV corresponds to Mo $3d_{3/2}$. Furthermore, the broad peak at 226.7 eV is assigned to the S 2s line.[41] The S 2p spectrum exhibits two peaks located at 161.9 eV and 161.5 eV that correspond to the sulphide (S^{2-}) group (Fig. 2G).[43,44] The peaks at 163.3 eV and 164.7 eV are assigned to the S $2p_{3/2}$ orbitals of S^{2-} and sulphite (S^{4+}).[45] The survey spectrum of C 1s

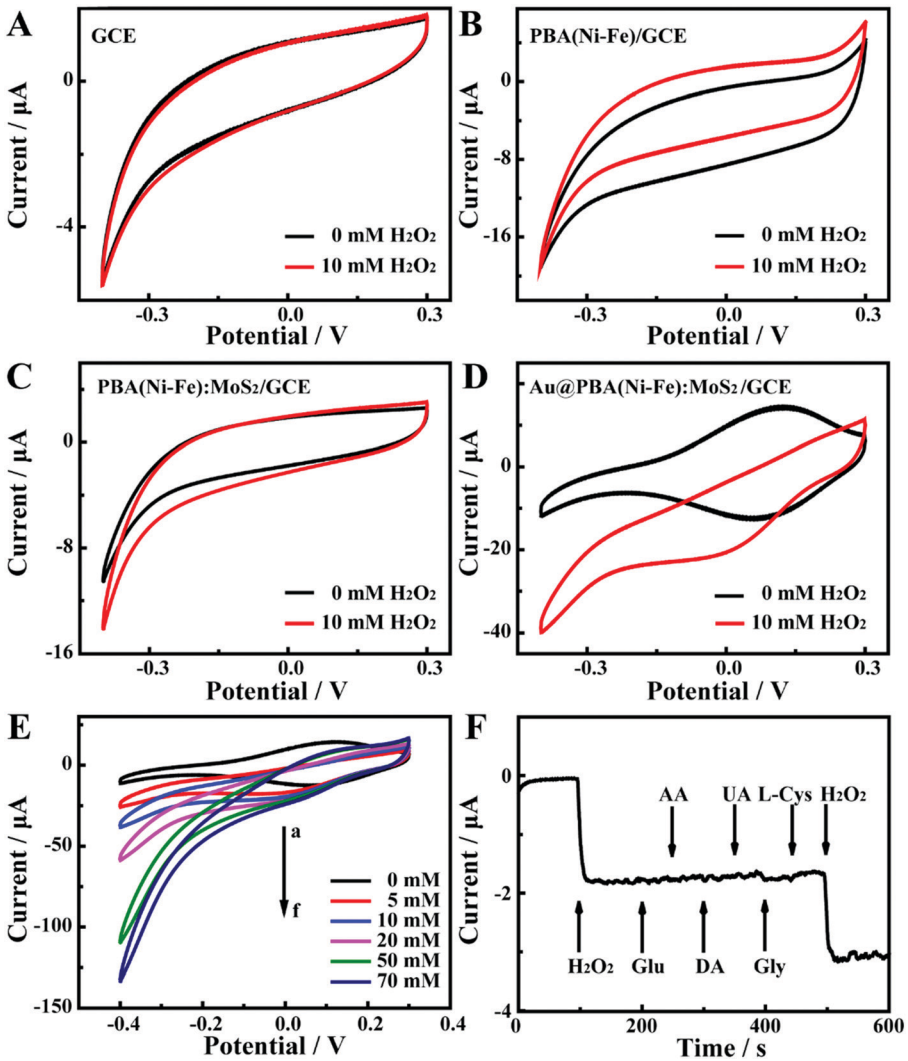

Fig. 3 Typical CV responses of (A) GCE, (B) PBA(Ni–Fe)/GCE, (C) PBA(Ni–Fe):MoS_2/GCE, and (D) Au@PBA(Ni–Fe):MoS_2/GCE in the presence of 0 mM and 10 mM H_2O_2 in 0.1 M PBS containing 0.1 M KCl (pH 7.4), scan rate: 100 mV s^{-1}, (E) CV curves of the Au@PBA(Ni–Fe):MoS_2/GCE electrode in 0.1 M PBS containing 0.1 M KCl (pH 7.4) containing 0, 5, 10, 20, 50 and 70 mM H_2O_2, (F) amperometric i–t response of Au@PBA(Ni–Fe):MoS_2/GCE in 0.1 M PBS containing 0.1 M KCl (pH 7.4) at an applied potential of 0 V with successive addition of 0.5 mM H_2O_2, 0.5 mM Glu, 0.1 mM AA, 0.1 mM DA, 0.1 mM UA, 0.1 mM Gly, and 0.1 mM L-cys and a second addition of 0.5 mM H_2O_2.

(Fig. 2H) displayed a main peak at 284.8 eV, which consisted of the C–N and C–C groups.[39]

FTIR and Raman spectroscopy were used to further verify the functional groups of the three nanocubes. As shown in Fig. S2A (ESI†), the three nanocubes possessed a strong absorption peak at 2090 cm^{-1}, which was caused by the stretching of the CN group in the Fe^{2+}–CN–Ni^{2+} section of the PBA.[33,46] For the three nanocubes, the peak at 1620 cm^{-1} and the broad peak at approximately 3480 cm^{-1} belonged to the O–H bending vibration modes.[47] For PBA(Ni–Fe), the peak at 2360 cm^{-1} was assigned to the C═O═C group of the CO_2 in air, while the peaks at 2922 cm^{-1} and 2852 cm^{-1} were ascribed to the C–H stretching absorptions of $–CH_2–$. Furthermore, in Fig. S2B (ESI†), the Raman specific peak at 2150 cm^{-1}, characteristic of the three nanocubes, was ascribed to the CN– stretching vibration of the PBA.[34] These data suggested that during the Au@PBA(Ni–Fe):MoS_2 formation, the cell structure remained unchanged. The Raman spectra also suggested that the combined Au nanoparticles influenced the electronic properties of MoS_2 (Fig. S2C, ESI†). The Au nanoparticles affected the S atoms' ability to undergo out-of-plane vibrations. The E2g and A1g peaks represent two vibrations of the S atoms in MoS_2. The S atoms opposite to a Mo atom experienced an in-plane vibration, and the S atoms moving in opposite directions accounted for the out-of-plane vibration.[47,48] Owing to the vibrations of the S atoms, the A1g mode was blue shifted.

Analytical performance of Au@PBA(Ni–Fe):MoS_2 nanocube-modified GCEs for *in vitro* detection of H_2O_2

Cyclic voltammetry (CV) is a common technique to investigate the catalytic performance of different materials. CV was used to detect the electrocatalytic capability towards H_2O_2 in 0.1 M phosphate buffer solution (PBS, pH = 7.4) containing 0.1 M KCl. Fig. 3 presents the CV curves for four electrodes

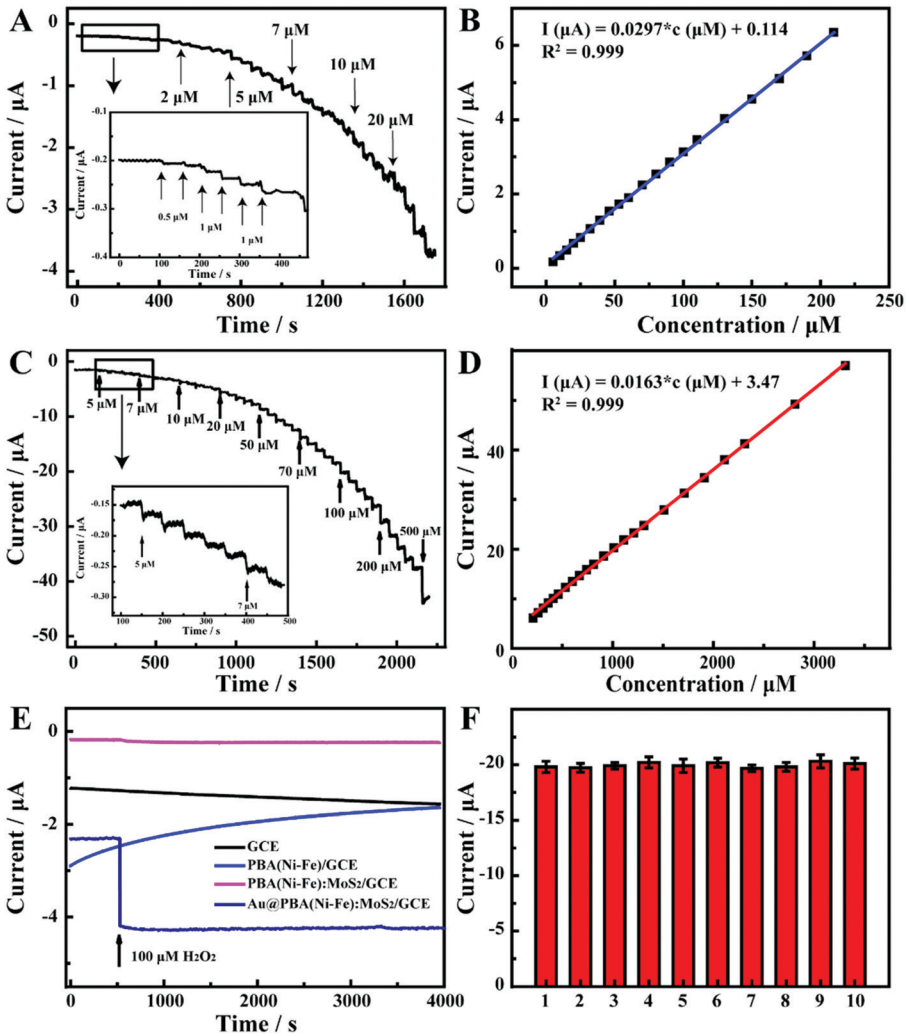

Fig. 4 Amperometric *i*–*t* responses of Au@PBA(Ni–Fe):MoS_2/GCE to the addition of different H_2O_2 concentrations ((A) 0.5 μM to 20 μM; (C) 5 μM to 500 μM) into 0.1 M PBS containing 0.1 M KCl (pH 7.4) under stirring; applied potential: 0 V. Calibration curves of the amperometric responses to the concentrations of H_2O_2 ((B) 0.5 μM to 200 μM; (D) 210 μM to 3000 μM). (E) Amperometric *i*–*t* response of the GCE, PBA(Ni–Fe)/GCE, PBA(Ni–Fe):MoS_2/GCE and Au@PBA(Ni–Fe):MoS_2/GCE in 0.1 M PBS containing 0.1 M KCl (pH 7.4) at an applied potential of 0 V with the addition of 100 μM H_2O_2. (F) Response current of 10 repetitive *i*–*t* of the same Au@PBA(Ni–Fe):MoS_2/GCE in 0.1 M PBS containing 0.1 M KCl (pH 7.4) with the addition of 1 mM H_2O_2.

with H_2O_2 concentrations of 0 mM and 10 mM. As seen from Fig. 3A and B, the GCE and PBA(Ni–Fe)/GCE yield the same electrocatalytic activity whether in the presence or absence of H_2O_2, while PBA(Ni–Fe):MoS_2/GCE produced a poor reduction current response in the presence of 10 mM H_2O_2 (Fig. 3C). However, under the same experimental conditions, Au@PBA(Ni–Fe):MoS_2/GCE showed a pair of redox peaks at approximately 0.15 V in the absence of H_2O_2 (Fig. 3D), which represented the conversion of Fe^{2+} and Fe^{3+}. Au nanoparticles significantly increased this response signal.[4] In the presence of H_2O_2, the reduction peak position moved to the left, and the reduction current increased significantly. The response current obtained with Au@PBA(Ni–Fe):MoS_2/GCE was 20 times that obtained with a bare GCE and 10 times that obtained with PBA(Ni–Fe)/GCE, which indicated that Au@PBA(Ni–Fe):MoS_2 nanocubes provided excellent electrocatalytic activity for H_2O_2 reduction. To confirm this effect, the GCEs were modified with the prepared nanocubes for EIS characterization. As shown in Fig. S3 (ESI†), Au@PBA(Ni–Fe):MoS_2 evidently exhibits a minimum R_{ct} value of approximately 220 Ω. The results show that Au can significantly improve the conductivity, which is beneficial to signal amplification.

Fig. 3E shows the different CV curves for Au@PBA(Ni–Fe):MoS_2/GCE when H_2O_2 is absent (curve a) and present (curve b–f) in 0.1 M PBS containing 0.1 M KCl. As the concentration of H_2O_2 increases, so does the cathode peak current value, gradually. The results indicate that Au@PBA(Ni–Fe):MoS_2 exhibits excellent electrocatalytic activity for reduction of H_2O_2. For biosensors, the ability to distinguish between target molecules and coexisting interfering molecules is important for the detection process. When detecting the H_2O_2 released from cells, the environment around the cells also contains Glu, AA, DA, UA and other biological molecules. As shown in Fig. 3F, the selectivity of Au@PBA(Ni–Fe):MoS_2/GCE is further displayed. The amperometric response of Au@PBA(Ni–Fe):MoS_2/GCE was tested by adding 0.5 mM H_2O_2, 0.5 mM Glu, 0.1 mM AA, 0.1 mM DA, 0.1 mM UA, 0.1 mM Gly and 0.1 mM L-cys as well as a second addition of 0.5 mM H_2O_2. Compared with H_2O_2, the responses to Glu, AA, DA, UA, Gly, and L-cys only resulted in insignificant currents during the detection. Consequently, Au@PBA(Ni–Fe):MoS_2/GCE exhibits good selectivity and can be used in complex physiological environments.

The sensitivity of Au@PBA(Ni–Fe):MoS_2/GCE towards H_2O_2 detection was also evaluated by amperometric *i–t* curves. Fig. 4A and C show the amperometric *i–t* response of Au@PBA(Ni–Fe):MoS_2/GCE to the continuous detection of varying concentrations of H_2O_2 at 0 V. During the detection, Au@PBA(Ni–Fe):MoS_2/GCE, because of the excellent electron transfer rate and electrocatalytic activity, demonstrated a rapid current response within 3 s when a certain amount of H_2O_2 was injected. As displayed in Fig. 4B and D, the change in reduction current was linear with respect to the H_2O_2 concentration from 0.5 μM to 200 μM and from 210 μM to 3000 μM, with a low detection limit of 0.23 μM (S/N = 3). The linear regression equation is found to be I (μA) = 0.0297 × c (μM) + 0.114 and I (μA) = 0.0163 × c (μM) + 3.47. Therefore, Au@PBA(Ni–Fe):MoS_2/GCE could be used as an electrochemical sensor to sensitively monitor H_2O_2.

Fig. 4E shows the long-term *i–t* responses to approximately 0.1 mM H_2O_2 for the four electrodes. After 1 h, Au@PBA(Ni–Fe):MoS_2/GCE retained the initial current response, whereas the other electrodes displayed higher or lower current variations. The results show that Au@PBA(Ni–Fe):MoS_2 has excellent stability. The amperometric *i–t* response was used to evaluate the repeatability of Au@PBA(Ni–Fe):MoS_2/GCE by injecting the same concentration of H_2O_2 (1 mM) into 0.1 M PBS containing 0.1 M KCl (pH 7.4) 10 times. Fig. 4F shows no clear decrease in the reduction current of H_2O_2, implying that Au@PBA(Ni–Fe):MoS_2/GCE possesses excellent reproducibility, wherein the calculated RSD value is approximately 1.24%. In a word, Au@PBA(Ni–Fe):MoS_2/GCE reveals admirable stability and repeatability to determine H_2O_2, which are essential features for a sensor in real-time applications. Compared with previously reported H_2O_2 sensors based on PB or other nanocubes, our detection method provides an improved performance, which can be seen in Table S1 (ESI†).

Detection of H_2O_2 released from living cells

H_2O_2 plays an important role in many biological processes, thus, it is essential to quantify H_2O_2 in the cellular environment. Au@PBA(Ni–Fe):MoS_2/GCE was used to detect the H_2O_2 released from living cancer cells. Artificial stimulation of the cells disrupts the intracellular redox homeostasis, causing H_2O_2 to flow out of the cells. HeLa cells were selected as the cells to be tested, and AA, as a stimulating factor, was used to stimulate cells into producing an abundance of H_2O_2.[49] AA was injected into PBS containing no cells and into another PBS fraction with cells and catalase, which served as control experiments. In the previous discussion (Section 3.2), AA did not generate a significant current response from Au@PBA(Ni–Fe):MoS_2/GCE at an applied voltage of 0 V (Fig. 4B). When AA was added to PBS containing ~4 × 10^6 cells, the cells released H_2O_2, and the current changed significantly. With time, H_2O_2 diffused into the solution, and the current value decreased (Fig. 5).

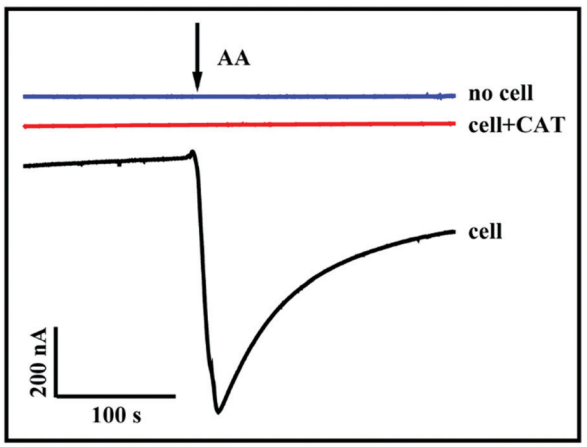

Fig. 5 Amperometric *i–t* responses of Au@PBA(Ni–Fe):MoS_2/GCE for the reduction of H_2O_2 released from HeLa cells in 0.1 M PBS containing 0.1 M KCl (pH 7.4) upon addition of 0.5 mM AA (the black line). The blue line is for the experiment without cells; the red line is for the experiment with HeLa cells and catalase.

Moreover, when AA was injected into PBS containing cells and catalase, the current remained almost unchanged. This result is consistent with that reported in the literature.[49] It is known that catalase can decompose H_2O_2, and the results show that the current change caused by the AA stimulation of cells results from H_2O_2 being released by cells.

Conclusions

In this study, Au@PBA(Ni–Fe):MoS_2 was synthesized by charge assembly and was implemented as a sensing material to detect H_2O_2. Due to the synergistic effect of Au nanoparticles and the PBA, the obtained Au@PBA(Ni–Fe):MoS_2 exhibited excellent electrical conductivity, the ability to catalyse H_2O_2 electrochemical reduction, and a sensitive detection of H_2O_2 at 0 V. With respect to H_2O_2 detection, the sensor provides a good performance, including a wide linear range as well as high stability and sensitivity. In addition, the H_2O_2 released from living cancer cells was successfully detected by Au@PBA(Ni–Fe):MoS_2/GCE. The observations of released H_2O_2 efflux indicate the presence of high levels of H_2O_2 in tumour cells. In the future, the developed sensor can be potentially used in cell biology, clinical diagnosis and pathophysiology.

Conflicts of interest

There are no conflicts to declare.

Acknowledgements

This work was financially supported by the National Natural Science Foundation (21575090), High-level Teachers in Beijing Municipal Universities in the Period of 13th Five-year Plan (CIT&TCD20190330), Scientific Research Project of Beijing Educational Committee (KM201810028008), Youth Innovative Research Team of Capital Normal University and Capacity Building for Sci-Tech Innovation-Fundamental Scientific Research Funds (19530050179, 025185305000/195).

References

1 L. Lin, T. Huang, J. Song, X. Y. Ou, Z. Wang, H. Deng, R. Tian, Y. Liu, J. F. Wang, Y. Liu, G. Yu, Z. Zhou, S. Wang, G. Niu, H. H. Yang and X. Chen, *J. Am. Chem. Soc.*, 2019, **141**, 9937–9945.
2 W. Lai, Z. Chen, J. Zhu, L. Yang, J. Zheng, X. Yi and W. Fang, *Nanoscale*, 2016, **8**, 3823–3833.
3 F. Luo, Y. Lin, L. Zheng, X. Lin and Y. Chi, *ACS Appl. Mater. Interfaces*, 2015, **7**, 11322–11329.
4 Y. Li, J. Cox and B. Zhang, *J. Am. Chem. Soc.*, 2010, **132**, 3047–3054.
5 Y. Ding, B. Yang, H. Liu, Z. Liu, X. Zhang, X. Zheng and Q. Liu, *Sens. Actuators, B*, 2018, **259**, 775–783.
6 Z. Bai, G. Li, J. Liang, J. Su, Y. Zhang, H. Chen, Y. Huang, W. Sui and Y. Zhao, *Biosens. Bioelectron.*, 2016, **82**, 185–194.
7 B. Ma, C. Kong, X. Hu, K. Liu, Q. Huang, J. Lv, W. Lu, X. Zhang, Z. Yang and S. Yang, *Biosens. Bioelectron.*, 2018, **106**, 29–36.
8 C. Dong, H. Zhong, T. Kou, J. Frenzel, G. Eggeler and Z. Zhang, *ACS Appl. Mater. Interfaces*, 2015, **7**, 20215–20223.
9 X. Jiang, H. Wang, R. Yuan and Y. Chai, *Anal. Chem.*, 2018, **90**, 8462–8469.
10 W. Jiang, L. Bai, M. Sang, M. Liu, S. Xuan, S. Wang and X. Gong, *J. Mater. Chem. B.*, 2019, **7**, 4568–4580.
11 F. Xie, X. Cao, F. Qu, A. M. Asiri and X. Sun, *Sens. Actuators, B*, 2018, **225**, 1254–1261.
12 B. Lu, X. Yuan, Y. Ren, Q. Shi, S. Wang, J. Dong and Z. D. Nan, *Bioelectrochemistry*, 2018, **123**, 103–111.
13 H. Dai, W. Lü, X. Zuo, Q. Zhu, C. Pan, X. Niu, J. Liu, H. Chen and X. Chen, *Biosens. Bioelectron.*, 2017, **95**, 131–137.
14 Y. Cui, F. Chen and X. B. Yin, *Biosens. Bioelectron.*, 2019, **125**, 208–215.
15 A. A. Karyakin, *Anal. Chem.*, 2017, **5**, 92–98.
16 L. Wang, Y. Han, X. Feng, J. Zhou, P. Qi and B. Wang, *Coord. Chem. Rev.*, 2016, **307**, 361–381.
17 R. Ojani, P. Hamidi and J. B. Raoof, *Chin. Chem. Lett.*, 2016, **27**, 481–486.
18 Z. Li, Y. Xin, W. Wu, B. Fu and Z. Zhang, *Anal. Chem.*, 2016, **88**, 7724–7729.
19 J. Nai and X. W. Lou, *Adv. Mater.*, 2018, 1706825.
20 L. Cui, J. Hu, C. C. Li, C. M. Wang and C. Y. Zhang, *Biosens. Bioelectron.*, 2018, **122**, 168–174.
21 Y. Ge, P. Dong, S. R. Craig, P. M. Ajayan, M. Ye and J. Shen, *Adv. Energy Mater.*, 2018, **8**, 1800484.
22 M. C. Radulescu, M. P. Bucur, B. Bucur and G. L. Radu, *Talanta*, 2019, **199**, 541–546.
23 M. A. Komkova, E. E. Karyakina and A. A. Karyakin, *J. Am. Chem. Soc.*, 2018, **140**, 11302–11307.
24 R. Li, X. Liu, W. Qiu and M. Zhang, *Anal. Chem.*, 2016, **88**, 7769–7776.
25 N. A. Sitnikova, A. V. Borisova, M. A. Komkova and A. A. Karyakin, *Anal. Chem.*, 2011, **83**, 2359–2363.
26 L. Chao, W. Wang, M. Dai, Y. Ma, L. Sun, X. Qin and Q. Xie, *J. Electroanal. Chem.*, 2016, **778**, 66–73.
27 L. Xiaxia, Z. Peiyao, L. Chunsen and P. Huan, *Chem. Commun.*, 2019, **55**, 9160–9163.
28 A. C. Amainath and S. N. Sawant, *Electrochim. Acta*, 2019, **295**, 294–301.
29 C. Lete, M. Marin, E. M. Anghel, L. Preda, C. Matei and S. Lupu, *Mater. Sci. Eng., C*, 2019, **102**, 661–669.
30 D. Jiang, C. Li, T. Liu, L. Li, Z. Chu, W. Jin and X. Ren, *Sens. Actuators, B*, 2017, **241**, 860–867.
31 J. Zhou, Y. Zhao, J. Bao, D. Huo, H. Fa, X. Shen and C. Hou, *Electrochim. Acta*, 2017, **250**, 152–158.
32 H. Shan, Q. Panzhe, F. Yunqi, L. Fuxiang, X. Xudong, Z. Chen, F. Qingmao and J. Baojiang, *Chem. – Asian J.*, 2019, **14**, 2259–2265.
33 D. Jiang, J. Pang, Q. You, T. Liu, Z. Chu and W. Jin, *Biosens. Bioelectron.*, 2019, **124**, 260–267.
34 X. Fang, J. Liu, J. Wang, H. Zhao, H. Ren and Z. Li, *Biosens. Bioelectron.*, 2017, **97**, 218–225.
35 L. Shi, Z. Chu, Y. Liu and W. Jin, *J. Mater. Chem.*, 2015, **3**, 3134–3140.

36 F. Sun, G. Wang, Y. Ding, C. Wang, B. Yuan and Y. Lin, *Adv. Energy Mater.*, 2018, **8**, 1800584.
37 A. Castan, S. Forel, L. Catala, I. Florea, F. Fossard, F. Bouanis, A. Andrieux-Ledier, S. Mazerat, T. Mallah, V. Huc, A. Loiseau and C. S. Cojocaru, *Carbon*, 2017, **123**, 583–592.
38 W. Lai, Z. Chen, J. Zhu, L. Yang, J. Zheng, X. Yi and W. Fang, *Nanoscale*, 2016, **8**, 3823–3833.
39 L. Shi, Y. Wang, S. Ding, Z. Chu, Y. Yin, D. Jiang, J. Luo and W. Jin, *Biosens. Bioelectron.*, 2017, **89**, 871–879.
40 H. K. Sadhanala, S. Senapati, K. V. Harika and K. K. Nanda, *New J. Chem.*, 2018, **42**, 14318–14324.
41 X. Dai, K. Du, Z. Li, M. Liu, Y. Ma, H. Sun, X. Zhang and Y. Yang, *ACS Appl. Mater. Interfaces*, 2015, **7**, 27242–27253.
42 L. Soler, A. Casanovas, A. Urrich, I. Angurell and J. Llorca, *Appl. Catal., B*, 2016, **197**, 47–55.
43 Y. Shu, J. Chen, Q. Xu, Z. Wei, F. Liu, R. Lu, S. Xu and X. Hu, *J. Mater. Chem.*, 2017, **5**, 1446–1453.
44 D. Jiang, Z. Chu, J. Peng and W. Jin, *Sens. Actuators, B*, 2016, **228**, 679–687.
45 E. Cato, A. Rossi, N. C. Scherrer and E. S. Ferreira, *J. Cult. Herit.*, 2018, **29**, 30–35.
46 V. B. Isfahani, N. Memarian, H. R. Dizaji, A. Arab and M. M. Silva, *Electrochim. Acta*, 2019, **304**, 282–291.
47 L. Liu, J. Wu, L. Wu, M. Ye, X. Liu, Q. Wang, S. Hou, P. Lu, L. Sun, J. Zheng, L. Xing, L. Gu, X. Jiang, L. Xie and L. Jiao, *Nat. Mater.*, 2018, **17**, 1108.
48 T. S. Sreeprasad, P. Nguyen, N. Kim and V. Berry, *Nano Lett.*, 2013, **13**, 4434–4441.
49 H. Chang, X. Wang, K. K. Shiu, Y. Zhu, J. Wang, Q. Li, B. Chen and H. Jiang, *Biosens. Bioelectron.*, 2013, **41**, 789–794.